Dissection of the NUP107 nuclear pore subcomplex reveals a novel interaction with spindle assembly checkpoint protein MAD1 in *Caenorhabditis elegans*

Eduardo Ródenas*, Cristina González-Aguilera, Cristina Ayuso, and Peter Askjaer
Centro Andaluz de Biología del Desarrollo, Consejo Superior de Investigaciones Científicas, Universidad Pablo de Olavide, Seville 41013, Spain

ABSTRACT **Nuclear pore complexes consist of several subcomplexes. The NUP107 complex is important for nucleocytoplasmic transport, nuclear envelope assembly, and kinetochore function. However, the underlying molecular mechanisms and the roles of individual complex members remain elusive. We report the first description of a genetic disruption of NUP107 in a metazoan. *Caenorhabditis elegans NUP107/npp-5* mutants display temperature-dependent lethality. Surprisingly, NPP-5 is dispensable for incorporation of most nucleoporins into nuclear pores and for nuclear protein import. In contrast, NPP-5 is essential for proper kinetochore localization of NUP133/NPP-15, another NUP107 complex member, whereas recruitment of NUP96/NPP-10C and ELYS/MEL-28 is NPP-5 independent. We found that kinetochore protein NUF2/HIM-10 and Aurora B/AIR-2 kinase are less abundant on mitotic chromatin upon NPP-5 depletion. *npp-5* mutants are hypersensitive to anoxia, suggesting that the spindle assembly checkpoint (SAC) is compromised. Indeed, NPP-5 interacts genetically and physically with SAC protein MAD1/MDF-1, whose nuclear envelope accumulation requires NPP-5. Thus our results strengthen the emerging connection between nuclear pore proteins and chromosome segregation.**

Monitoring Editor
Martin Hetzer
Salk Institute for Biological Studies

Received: Nov 17, 2011
Revised: Dec 28, 2011
Accepted: Jan 6, 2012

INTRODUCTION

The nuclear pore complex (NPC) is a macrostructure within the nuclear envelope (NE) composed of multiple copies of ~30 different proteins called nucleoporins (Nups; Hetzer and Wente, 2009). NPCs are estimated to have a total molecular weight of ~50–60 MDa (Rout *et al.*, 2000; Cronshaw *et al.*, 2002; Alber *et al.*, 2007), and they serve as the only known transport route of RNA and protein between the nucleus and the cytoplasm. In addition, it is becoming increasingly clear that Nups have a determinant role in regulation of gene expression (Capelson *et al.*, 2010; Kalverda *et al.*, 2010; Strambio-De-Castillia *et al.*, 2010). Nups interact with each other to form subcomplexes in some cases, such as the NUP93/205/188 complex that regulates the NPC permeability barrier and passage of membrane proteins through the NPC (Grandi *et al.*, 1997; Galy *et al.*, 2003; Theerthagiri *et al.*, 2010). Another example is the NUP107 complex, which is composed of nine different Nups (NUP37, NUP43, NUP85, NUP96, NUP107, NUP133, NUP160, SEH1, and SEC13) in vertebrates. The NUP107 complex is biochemically stable, and its purification from the yeast *Saccharomyces cerevisiae* revealed that it adopts a Y-shaped structure (Siniossoglou *et al.*, 2000). Within this Y-shaped structure Nup84p, the yeast orthologue of NUP107, interacts with Nup133p at the bottom tip of the Y and with Nup145Cp/NUP96 + Sec13p further up the stalk (Lutzmann *et al.*, 2002). Whereas several members of the yeast Nup84p complex, including Nup84p itself (Siniossoglou *et al.*, 1996), are dispensable for growth, studies in vertebrates demonstrated that the NUP107 complex is critical for postmitotic and interphase NPC formation (Boehmer *et al.*, 2003; Harel *et al.*, 2003;

This article was published online ahead of print in MBoC in Press (http://www.molbiolcell.org/cgi/doi/10.1091/mbc.E11-11-0927) on January 11, 2012.

*Present address: Program in Gene Function and Expression, University of Massachusetts Medical School, Worcester, MA 01605.

Address correspondence to: Peter Askjaer (pask@upo.es).

Abbreviations used: CPC, chromosomal passenger complex; NE, nuclear envelope; NPC, nuclear pore complex; Nup, nucleoporin; PTC, premature termination codon; SAC, spindle assembly checkpoint.

Walther *et al.*, 2003; D'Angelo *et al.*, 2006). Moreover, depletion of the NUP107 complex from *Xenopus laevis* egg extracts prevents efficient spindle assembly (Orjalo *et al.*, 2006). On entry into mitosis the entire subcomplex localizes to kinetochores (Belgareh *et al.*, 2001; Loiodice *et al.*, 2004). Kinetochores are conserved structures composed of >80 proteins and link spindle microtubules to chromosomes to segregate DNA during anaphase (Cheeseman and Desai, 2008). Kinetochores are composed of three main layers: the inner kinetochore, which interacts with centromeric DNA; the outer kinetochore, which constitutes the surface of interaction with spindle microtubules; and the central kinetochore, which is the region between the inner and outer kinetochore. It was recently demonstrated that the localization of the NUP107 complex to kinetochores is dependent on NDC80 and CENP-F, two outer kinetochore components, and that NUP133 interacts directly with CENP-F (Zuccolo *et al.*, 2007).

The spindle assembly checkpoint (SAC) is a mitotic control mechanism that ensures that chromosomes do not segregate until they are properly bioriented and attached to microtubules (Tanaka, 2010). If a kinetochore is not attached to spindle microtubules, the SAC delays anaphase onset by sequestering CDC20, an activator of the anaphase-promoting complex/cyclosome (APC/C; Fang *et al.*, 1998). The APC/C is an E3 ubiquitin ligase that targets key mitotic substrates for degradation, such as cyclin B and securin. The SAC is also involved in detection of lack of stretch-induced tension between kinetochores on sister chromatids (Maresca and Salmon, 2009; Uchida *et al.*, 2009; Wan *et al.*, 2009). In the absence of tension, Aurora B, a member of the chromosomal passenger complex (CPC) that localizes at the inner centromere, phosphorylates NDC80 and other kinetochore proteins. This reduces the stability of microtubule–kinetochore interactions, thus signaling to the SAC due to an unbound kinetochore situation (Lampson and Cheeseman, 2011). Of interest, it has been shown that SEH1, a member of the NUP107 complex, regulates the centromeric localization of Aurora B and other CPC proteins (Platani *et al.*, 2009). When proper attachment of spindle microtubules to kinetochore occurs, provoking tension between sister chromatids, the SAC is satisfied and mitosis can progress.

In this article, we characterize a *NUP107*-null mutation in *Caenorhabditis elegans*. Targeting of single NUP107 subcomplex members by RNA interference (RNAi) in mammalian cells or by immunodepletion from cell-free extracts frequently causes an efficient codepletion of most other subcomplex members (Boehmer *et al.*, 2003; Harel *et al.*, 2003; Walther *et al.*, 2003), which has prevented assignation of specific functions to individual proteins. However, we find that expression of all *C. elegans* Nups tested, except for NUP133/NPP-15, is unaffected by the removal of NUP107/NPP-5, making the nematode an attractive model with which to study the function of NUP107 complex components (Table 1). Unexpectedly, we observe that NPCs assemble and function in the absence of NPP-5, whereas NPP-5 localization is highly sensitive to depletion of other NUP107 complex members. We also show that kinetochore assembly is partially inhibited in *npp-5* mutants and that NPP-5 binds to and regulates NE accumulation of MAD1/MDF-1, a member of the SAC. Depletion of MDF-1 in *npp-5* mutants leads to high synthetic embryonic lethality, suggesting that the SAC is required for cell viability in the absence of NPP-5.

C. elegans protein	Human orthologue
AIR-2	Aurora B
BUB-3	BUB3
CYB-3	Cyclin B3
HIM-10	NUF2
MDF-1	MAD1
MDF-2	MAD2
MEL-28	ELYS
MIS-12	MIS12
NPP-2	NUP85
NPP-5	NUP107
NPP-6	NUP160
NPP-7	NUP153
NPP-8	NUP155
NPP-10N	NUP98
NPP-10C	NUP96
NPP-15	NUP133
NPP-18	SEH1
NPP-19	NUP35
NPP-23	NUP43
SAN-1	BUBR1

TABLE 1: Overview of genes involved in this study.

RESULTS

NUP107/NPP-5 is required for proper development

To evaluate the implication of NUP107 in animal development, we characterized two mutant alleles of the *C. elegans* orthologue of NUP107, encoded by the *npp-5* gene (standard *C. elegans* nomenclature is used hereafter; see Table 1). Allele *npp-5*(*tm3039*) is a 524–base pair deletion from the first intron to the fourth exon, whereas 1291 base pairs from the fourth exon to the sixth exon are deleted in allele *npp-5*(*ok1966*) (Figure 1A). Reverse transcription (RT)–PCR revealed the activation of a cryptic 3′ splice site in *npp-5*(*tm3039*), which creates a premature termination codon (PTC) after 35 amino acid residues (Supplemental Figure S1), implying that *npp-5*(*tm3039*) is a null allele. The deletion in *npp-5*(*ok1966*) similarly induces a PTC downstream of the mutation, but in this case approximately one-third of the open reading frame is intact (Supplemental Figure S1). We raised an antibody against a peptide from the N-terminus of NPP-5. As expected from the molecular lesion, neither Western blotting (Figure 1B) nor immunofluorescence analysis (Figure 1C) revealed a specific signal in *npp-5*(*tm3039*) mutants. The absence of signal in *npp-5*(*ok1966*) mutants suggested that the PTC renders the mRNA unstable. Both mutants can be propagated as homozygous strains; however, we introduced a balancer chromosome into each strain to avoid selection for suppressor mutations or epigenetic changes. Adult offspring from heterozygous animals consisted of 26.2–26.7% homozygous mutants (*npp-5*(*ok1966*), n = 806; *tm3039*, n = 757), indicating that maternal contribution of NPP-5 enables mutants to complete embryonic and larval development. Analyzing brood size of F1 homozygous mutants revealed a decrease of 21.9% in *npp-5*(*ok1966*) and 33.4% in *npp-5*(*tm3039*) (Table 2; $p < 0.005$). For both alleles we observed a low but statistically significant increase in the frequency of lethality among F2 embryos produced by F1 homozygous mutants (Table 2; 5.3–7.3%). F2 larval development was severely compromised in both mutants, with only 8.9–12.0% of the offspring developing into adults at 20°C (Figure 1D). At 25°C no offspring developed into fertile adults,

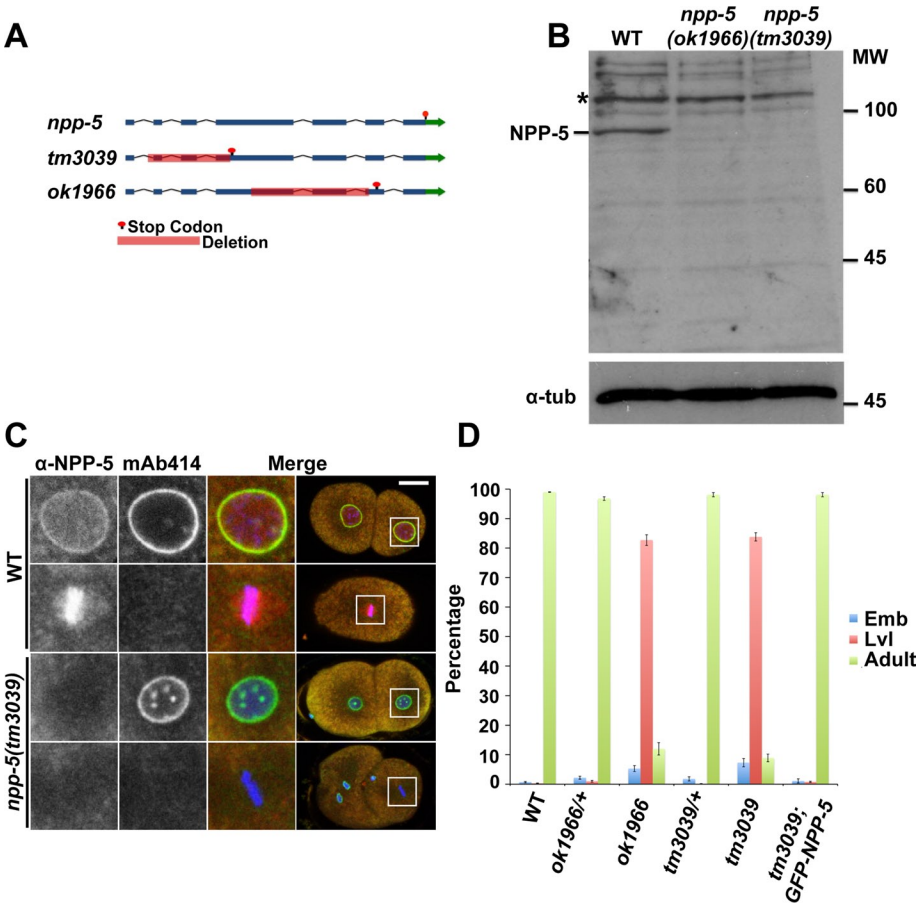

FIGURE 1: *npp-5(tm3039)* and *npp-5(ok1966)* are null mutations of *NUP107/npp-5*. (A) Schematic representation of the *C. elegans npp-5* gene and deletion alleles *npp-5(ok1966)* and *npp-5(tm3039)*. Exons and introns are indicated by boxes and lines, respectively. (B) Western blot analysis of ~1500 wild-type (WT), *npp-5(ok1966)*, and *npp-5(tm3039)* embryos probed with anti-NPP-5 and anti–α-tubulin antibodies. NPP-5 appeared with a molecular weight of ~92 kDa in wild-type embryos only. Asterisk indicates nonspecific cross-reactivity. (C) Wild type and *npp-5(tm3039)* embryos were fixed and stained with anti–NPP-5 antiserum (red) and monoclonal antibody mAb414 (green). Chromatin was detected using Hoechst 33258 (blue). Boxed regions in the merged panels are shown at higher magnification to the left. Scale bar, 10 μm. (D) Percentage of wild-type, *npp-5(ok1966)* and *npp-5(tm3039)* offspring dying during embryogenesis (Emb) or larval development (Lvl) or reaching adulthood (Adult) at 20°C. Error bars, SE of the mean.

suggesting a higher requirement for NPP-5 when developmental pace is increased (Table 2). Of importance, ectopic expression of green fluorescent protein (GFP)–NPP-5 fully restored embryonic and larval development of *npp-5(ok1966)* and *npp-5(tm3039)* mutants (Table 2 and Figure 1D). This observation, together with the identical behavior of the two mutant alleles, confirmed that the observed phenotypes could be attributed to the *npp-5* gene. We therefore conclude that NPP-5 plays a critical role in *C. elegans* development.

NPP-5 is dispensable for nuclear protein import

The developmental arrest could potentially reflect defects in NE function, including nucleocytoplasmic transport. To test this, we monitored the growth rate of P1 cell nuclei following the first mitosis in embryos expressing GFP fused to histone H2B/HIS-58 (Figure 2A). Whereas nuclei in embryos produced by heterozygous siblings (which are referred to as control embryos hereafter) grew by 0.56 ± 0.02 $\mu m^3/s$ (time interval 152–696 s after anaphase onset; n = 12), the rate was reduced to 0.42 ± 0.02 $\mu m^3/s$ in F2 mutant embryos (n = 13; 25.6% decrease, $p < 2 \times 10^{-5}$). The final size of P1 nuclei was reduced by 12.8% ($p < 0.05$). In both control and *npp-5(tm3039)* embryos P1 nuclei kept growing until entry into mitosis, which occurred after ~832 s in control and ~880 s in mutant embryos. Thus absence of NPP-5 reduced nuclear growth and delayed entry into mitosis.

Structural changes in NPCs can affect NE permeability. Inert molecules larger that ~45 kDa are normally unable to cross the NE, but depletion of Nups can increase this permeability barrier. We investigated whether this was also the case in *npp-5(tm3039)* embryos by injecting the gonad arms of hermaphrodites with a mixture of fluorescent dextrans (Galy *et al.*, 2003). We observed that 70- and 155-kDa dextrans were effectively excluded from nuclei from both control and *npp-5(tm3039)* embryos, indicating that the permeability barrier was not grossly affected in the absence of NPP-5 (Figure 2B). Next we monitored nuclear accumulation of several protein substrates fused to GFP. PIE-1 is a transcriptional regulator found specifically in germline blastomeres, where it is imported into the nucleus by an unknown transport pathway (Reese *et al.*, 2000). In both control and *npp-5(tm3039)* four-cell-stage embryos robust nuclear accumulation of PIE-1–GFP was observed in the P2 cell, although time-course analysis indicated a trend for slower import in the absence of NUP107 (Figure 2C and Supplemental Movie S1; $p = 0.40$). Similarly, stress-induced nuclear import of the transcription factor DAF-16, as well as constitutive nuclear import of lacZ-GFP coupled to the SV40 T-antigen nuclear localization signal in intestine and vulva cells, was observed in *npp-5* mutants (Supplemental Figure S2, A and B). We therefore concluded that NPP-5 is dispensable for importin α/β–mediated nuclear protein import, but we cannot rule out that nucleocytoplasmic transport of other substrates may be NPP-5 dependent.

NPC assembly can occur in the absence of NPP-5

The NUP107 complex is essential for postmitotic and interphase NPC assembly (Harel *et al.*, 2003; Walther *et al.*, 2003; D'Angelo *et al.*, 2006), but the relative contribution of each member of the subcomplex has remained largely unknown, partly because small interfering RNA (siRNA) approaches in vertebrate cells lead to a general down-regulation of most or all components. To address the issue of coregulation, embryonic extracts from wild-type and *npp-5(tm3039)* animals were analyzed by Western blotting using antibodies against NUP96/NPP-10C and NUP133/NPP-15 from the NUP107 complex, as well as NUP35/NPP-19, NUP98/NPP-10N, and NUP153/NPP-7. Except for NPP-15, all these Nups were present at normal levels in *npp-5(tm3039)* embryos (Figure 3A and Supplemental Figure S3). Moreover, we previously showed that knockdown of NPP-5 does not affect expression of ELYS/MEL-28 in *C. elegans* (Galy *et al.*, 2006). Conversely, RNAi against *npp-19* (Rodenas *et al.*,

Genotype	n[a]	Brood size	Embryonic lethality (%)	Larval lethality (%)	Adults (%)
Wild type, 20°C	6	319 ± 6	0.7 ± 0.2	0.3 ± 0.1	99.0 ± 0.1
Wild type, 25°C	3	217 ± 25	1.8 ± 1.0	0.2 ± 0.2	98.0 ± 1.1
ok1966/+, 20°C	5	273 ± 10†	2.2 ± 0.5	1.0 ± 0.3	96.8 ± 0.6
ok1966, 20°C	6	249 ± 15†	5.3 ± 1.0*	82.7 ± 1.8*	12.0 ± 2.1*
tm3039/+, 20°C	5	257 ± 11†	1.8 ± 0.7	0.1 ± 0.1	98.1 ± 0.7
tm3039, 20°	10	212 ± 14†	7.3 ± 1.4*	83.8 ± 1.4*	8.9 ± 1.3*
tm3039; GFP-NPP-5, 20°C	9	259 ± 19	1.1 ± 0.7	0.8 ± 0.2	98.1 ± 0.7
tm3039, 25°C	4	145 ± 14†	18.2 ± 4.1*	81.8 ± 4.1*	0.0 ± 0.0*

Heterozygous or first-generation homozygous mutant L4 hermaphrodites were incubated on nematode growth medium plates at indicated temperatures and moved to fresh plates every 8–16 h. Wild-type N2 strain was used as control.
[a]Number of founders. For each founder, brood sizes and the percentages of embryonic lethality, arrested or dead larvae, and adults were determined after 0, 24, and 96 h (average ± SE of the means).
†Significant differences by two-tailed *t* test: different from the wild type at same temperature ($p < 0.005$).
*Significant differences by chi-square test: different from the wild type at same temperature ($p < 0.001$).

TABLE 2: Development of *npp-5(ok1966)* and *npp-5(tm3039)* mutants.

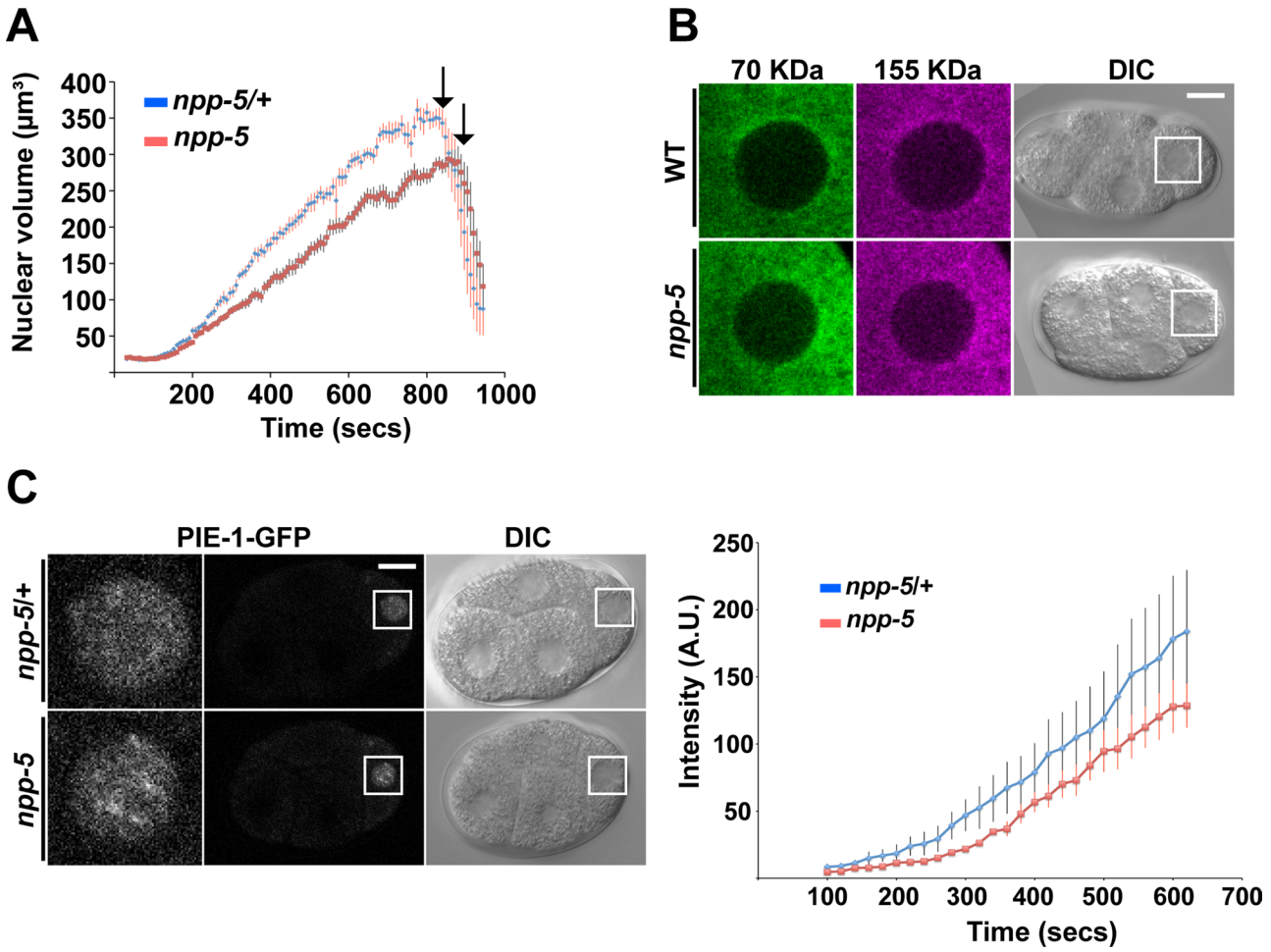

FIGURE 2: Nuclear protein import occurs in the absence of NPP-5. (A) Size of P1 nuclei was determined by time-lapse microscopy, revealing a significantly slower nuclear growth rate in *npp-5(tm3039)* embryos (n = 13) compared with *npp-5(tm3039)/+* embryos (n = 12). Time is relative to P0 anaphase onset. (B) Gonads of wild-type (n = 14) and *npp-5(tm3039)* (n = 16) animals were injected with a mixture of 70- (green) and 155-kDa (magenta) dextrans. Exclusion of the dextrans from embryonic nuclei was observed by live confocal microscopy. (C) Nuclear import of PIE-1-GFP into P2 nuclei was observed by time-lapse microscopy (left) and quantified (right). Import in *npp-5(tm3039)* embryos (n = 10) was comparable to that in control embryos (n = 10). Time is relative to P1 anaphase onset. Error bars, SE of the mean. Scale bars, 10 µm.

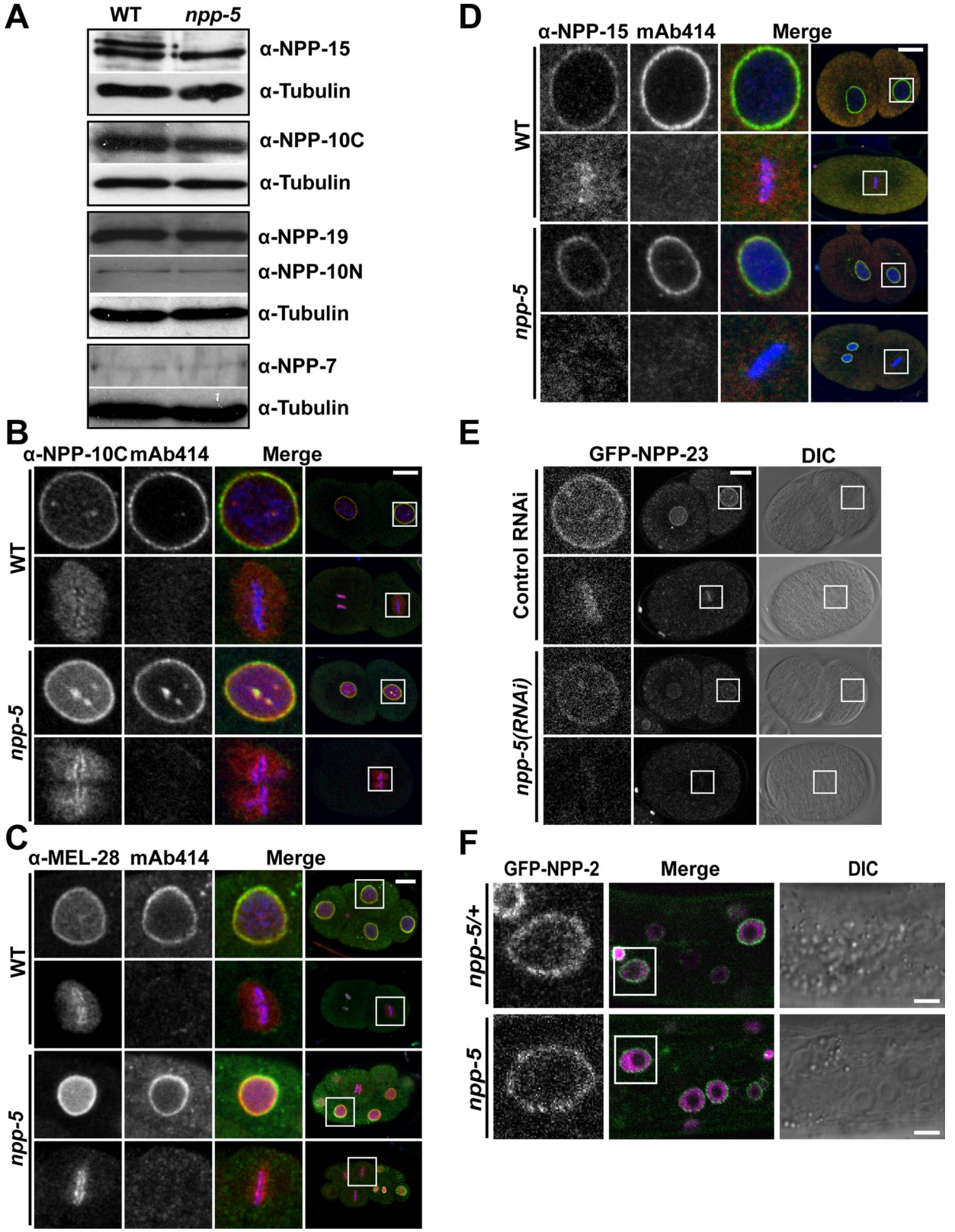

FIGURE 3: Expression and localization of most Nups are NPP-5 independent. (A) Western blot analysis of embryonic extracts showed similar expression levels of NPP-7, NPP-10N, NPP-10C, and NPP-19 in *npp-5(tm3039)* embryos compared with the wild type. In contrast, NPP-15 appeared as a duplet in the wild type but not in the mutant. (B–D) Wild type, *npp-5(tm3039)* (B, D), and *npp-5(ok1966)* (C) embryos were fixed and stained with serum against NPP-10C (B), MEL-28 (C), or NPP-15 (D) (red) and mAb414 (green). Chromatin was detected using Hoechst 33258 (blue). (E, F) Expression of GFP-NPP-23 and GFP-NPP-2/mCherry-HIS-58 was analyzed by live microscopy. Whereas depletion of NPP-5 inhibited recruitment of GFP-NPP-23 ($n \geq 24$ for each treatment; E), GFP-NPP-2 was unaffected (F; $n \geq 8$ for each treatment). Boxed regions in the merged panels are shown at higher magnification to the left. Scale bars, 10 μm.

2009), NUP155/*npp-8* (Franz *et al.*, 2005), or *mel-28* (Galy *et al.*, 2006) was shown not to affect expression of NPP-5. The independent expression of individual Nups tested so far underlines the usefulness of *C. elegans* as genetic system to dissect the function of NPC components (Gorjanacz *et al.*, 2007). Affinity-purified antibodies against NPP-15 gave rise to two bands of the expected size (~128 kDa) in wild-type extracts but, intriguingly, only a single band in *npp-5(tm3039)* (Figure 3A). Comparing extracts from wild-type embryos to extracts from embryos produced by animals heterozygous for a *npp-15* deletion allele (*ok1954*) showed that both bands correspond to NPP-15 protein (Supplemental Figure S3F).

We next analyzed whether the lack of NPP-5 prevented proper localization of components of the NUP107 complex. MEL-28 and NPP-10C localized at the nuclear periphery in interphase and to kinetochores during mitosis in both wild-type and *npp-5(tm3039)* embryos (Figure 3, B and C). Moreover, the monoclonal antibody mAb414, a general NPC marker, showed normal staining in the absence of NPP-5. Nuclear rim accumulation of NPP-15 was similarly unaffected by NPP-5 depletion (Figure 3D). However, recruitment to kinetochores in mitosis was detected only in wild-type embryos but not in *npp-5(tm3039)* embryos. To investigate additional members of the NUP107 complex, we made transgenic strains expressing GFP fused to either NUP43/NPP-23 (D'Angelo *et al.*, 2009) or NUP85/NPP-2, neither of which had been visualized previously in *C. elegans*. As expected, both Nups localized to NPCs and kinetochores in the wild type (Figure 3, E and F; and data not shown). Whereas nuclear rim and kinetochore recruitment of GFP-NPP-23 was diminished in embryos depleted for NPP-5 by RNAi (Figure 3E), GFP-NPP-2 was present at normal levels at the nuclear periphery in *npp-5(tm3039)* animals (Figure 3F). Our GFP-NPP-2 reporter was only expressed in postembryonic cells, which precluded a detailed analysis of mitosis in second-generation mutants since divisions have largely ceased in these animals. In first-generation mutants at the larval L2–L3 stage GFP-NPP-2 localized to kinetochores during division of seam cells (data not shown), but we cannot exclude the presence of low amounts of maternally contributed NPP-5 protein in these animals. We conclude that in the absence of NPP-5 only localization of NPP-23 and NPP-15 is affected, suggesting that NPC assembly and stability of the NUP107 complex are largely NPP-5 independent.

Localization of NPP-5 depends on most other subcomplex members

Having observed that most Nups behave normally in NPP-5-depleted animals, we asked the reciprocal question: which members of the NUP107 complex are required to properly localize NPP-5? Using the rescuing GFP-NPP-5 strain (Table 2), we analyzed NPP-5 dynamics in control and RNAi-treated embryos. On depletion of NPP-2, the signal of GFP-NPP-5 was reduced both at the nuclear periphery and at kinetochores, whereas RNAi against *npp-10C* and NUP160/*npp-6* completely abolished NPP-5 recruitment (Figure 4 and Supplemental Movies S2–S5). Targeting *npp-10C* caused, moreover, severe chromosome segregation defects in mitosis. Because NPP-10N and NPP-10C are translated as a precursor polypeptide from a common mRNA, RNAi efficiently knocks down expression of both Nups (Galy *et al.*, 2003). Thus these phenotypes might contribute to the lack of NPP-10N, NPP-10C, or both. Analyzing endogenous NPP-5 by immunofluorescence confirmed the dependence on NPP-2, NPP-10N/C, NPP-6, and MEL-28 for correct localization of NPP-5 (Supplemental Figure S4). In contrast, we found that RNAi against SEH1/*npp-18* did not impede recruitment of NPP-5. Together these results suggest that whereas the NUP107 complex is stable in the absence of NPP-5, NUP107/NPP-5 itself is very sensitive to perturbations of the NPC subcomplex.

NPP-5 is required for proper kinetochore assembly and Aurora B/AIR-2 recruitment

The mitotic localization of the NUP107 complex to kinetochores led to the hypothesis that Nups could be directly involved in chromosome segregation (Belgareh *et al.*, 2001). In support of this, HeLa cells with reduced NUP107 and SEH1 loading onto kinetochores showed increase frequency of misaligned chromosomes during metaphase (Zuccolo *et al.*, 2007). To test whether depletion of NPP-5 affects kinetochore assembly in *C. elegans*, we monitored the behavior of outer kinetochore proteins NUF2/HIM-10 and MIS12/MIS-12, which are members of the NDC80 and MIS12 complexes, respectively. Quantification of GFP-HIM-10 at kinetochores of metaphase chromosomes revealed a 39% reduction in *npp-5(tm3039)* embryos (Figure 5A and Supplemental Movie S6; $p < 0.01$), whereas GFP-MIS-12 localization was NPP-5 independent (Figure 5B and Supplemental Movie S7; $p \approx 0.62$). These results suggest that NPP-5 is required for specific aspects of outer kinetochore assembly.

The fidelity of bipolar microtubule attachment to kinetochores is monitored by the CPC, which includes INCENP, Survivin, Borealin, and the protein kinase Aurora B. We tested whether CPC recruitment is NPP-5 dependent by measuring GFP-Aurora B/AIR-2 levels on mitotic chromatin. This revealed a 34% reduction of chromatin-associated GFP-AIR-2 during metaphase in *npp-5(tm3039)* embryos as compared with control embryos (Figure 5C and Supplemental Movie S8; $p < 0.01$). Thus we concluded that NPP-5 is required for proper localization of specific kinetochore and CPC components.

Spindle assembly checkpoint protein MAD1/MDF-1 accumulates at kinetochores in the absence of NPP-5

Unattached kinetochores due either to defective kinetochore assembly or Aurora B–mediated correction of syntelic and merotelic microtubule (MT)–kinetochore attachments are detected by the SAC (Tanaka, 2010; Lampson and Cheeseman, 2011). On the basis of our observation that HIM-10 and AIR-2 localization is partially compromised in *npp-5(tm3039)* embryos, we addressed two questions: Does the absence of NPP-5 from kinetochores trigger a signal to the SAC? Is the SAC functional in cells lacking NPP-5? To answer the first question, we investigated whether SAC proteins MAD1/MDF-1 and MAD2/MDF-2 localize to mitotic chromatin in *npp-5(tm3039)* embryos. In contrast to the situation in most vertebrate cells, *C. elegans* MDF-1 and MDF-2 accumulate on chromatin only if cells are stressed during mitosis (Yamamoto *et al.*, 2008; Essex *et al.*, 2009). Live recordings of *npp-5(RNAi)* embryos revealed faint but reproducible accumulation of GFP-MDF-1 on chromatin during metaphase, suggesting that absence of NPP-5 is detected by the SAC (Figure 6A and Supplemental Movie S9). GFP-MDF-2 recruitment was not observed, however, possibly due to a strong fluorescence signal from soluble protein (Supplemental Figure S5A). We next induced a situation of massive monotelic and syntelic MT–kinetochore attachment by preventing centrosome duplication through RNAi-mediated loss of ZYG-1 protein (Yamamoto *et al.*, 2008; Essex *et al.*, 2009). As previously shown, SAC proteins strongly accumulated on mitotic chromatin of two-cell-stage *zyg-1(RNAi)* embryos (Figure 6B and Supplemental Figure S5B). Because depletion of NPP-5 did not interfere with localization of GFP-MDF-1 or GFP-MDF-2 in *zyg-1(RNAi)* embryos (Figure 6B and Supplemental Figure S5B), we conclude that NPP-5 is not required for robust SAC signaling upon strong stimuli, such

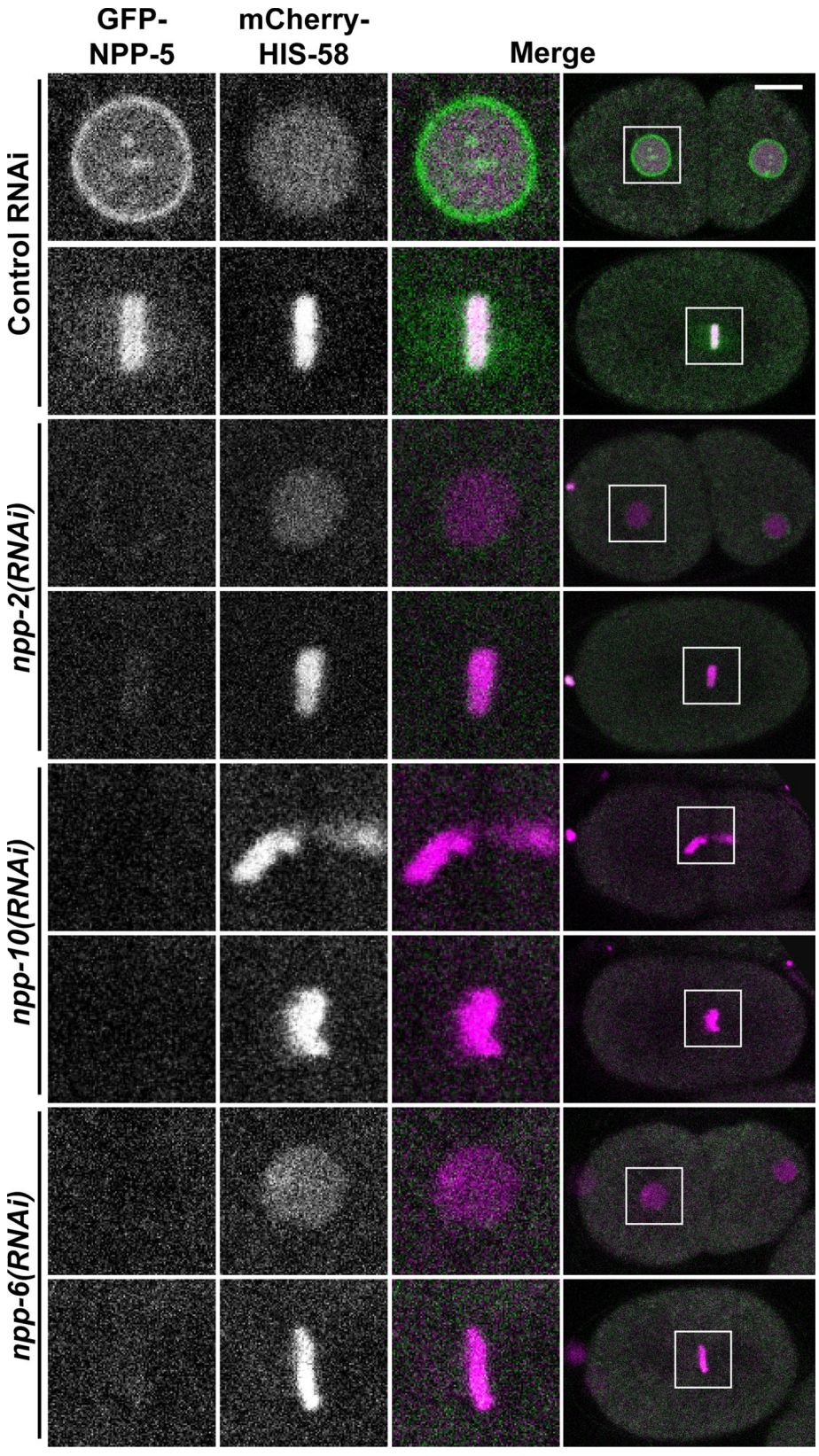

FIGURE 4: NPP-5 localization is sensitive to perturbations of other NUP107 complex members. Still images from time-lapse confocal microscopy of embryos expressing GFP-NPP-5 (green) and mCherry-HIS-58 (magenta). RNAi against *npp-2*, *npp-10*, or *npp-6* inhibited proper localization of GFP-NPP-5 during interphase (top rows) and metaphase (bottom rows; $n \geq 8$ for each treatment). Boxed regions on the right are shown at higher magnification to the left. Scale bar, 10 μm.

as monopolar spindle formation. Similarly, the NUP107 complex is not required for SAC function in cell-free *Xenopus* extracts (Orjalo *et al.*, 2006).

MDF-1 localizes to NPCs through NPP-5

Initially described in budding yeast, Mad1p and to some degree also Mad2p accumulate at NPCs in several cell types during interphase (Campbell *et al.*, 2001; Iouk *et al.*, 2002). In interphase cells of *C. elegans* embryos, GFP-MDF-1 also showed enhanced signal at the NE in addition to diffuse nucleoplasmic staining (Figure 6C). It is striking that the NE accumulation of GFP-MDF-1 was absent in NPP-5–depleted embryos, whereas the intranuclear signal was normal (Figure 6C and Supplemental Movie S9). Immunofluorescence analysis of endogenous MDF-1 in control and *npp-5(tm3039)* embryos confirmed these observations (Figure 6D), demonstrating that NPP-5 is strictly required to localize MDF-1 to the NE.

To investigate whether MDF-1 accumulates at NPCs via a physical interaction with NPP-5, we expressed the two proteins in budding yeast, fused to either the Gal4 activation domain or the Gal4 DNA-binding domain. Only when MDF-1 and NPP-5 fusion proteins were expressed simultaneously did the yeast grow on media lacking the selectable markers histidine and adenine (Figure 7, top), indicating that the two proteins interact directly. Because budding yeast Mad1p and Nup53p have been demonstrated to interact physically (Scott *et al.*, 2005), we also tested whether this was the case for the *C. elegans* orthologues MDF-1 and NPP-19. However, we did not observe any interaction in the yeast-two-hybrid assay (Figure 7, bottom), which suggests that MAD1 is anchored at the NPC in a species-specific manner.

NPP-5–deficient embryos are hypersensitive to MDF-1 perturbation

Our observation that NPP-5 is partially responsible for MDF-1 localization prompted us to investigate whether they interact genetically. Indeed, we found that whereas depletion of the proteins singly caused only 3–5% embryonic lethality, RNAi against *mdf-1* in *npp-5(tm3039)* animals led to 85 ± 7% embryonic lethality (Figure 8A; $p < 0.001$). MDF-2, which forms a complex with MDF-1, showed an intermediate degree of synthetic embryonic lethality with NPP-5 (32 ± 6%; $p < 0.001$), whereas depletion of SAC protein BUBR1/SAN-1 or BUB3/BUB-3 did not enhance lethality in *npp-5(tm3039)* embryos ($p > 0.10$). Thus NPP-5 displays a synthetic

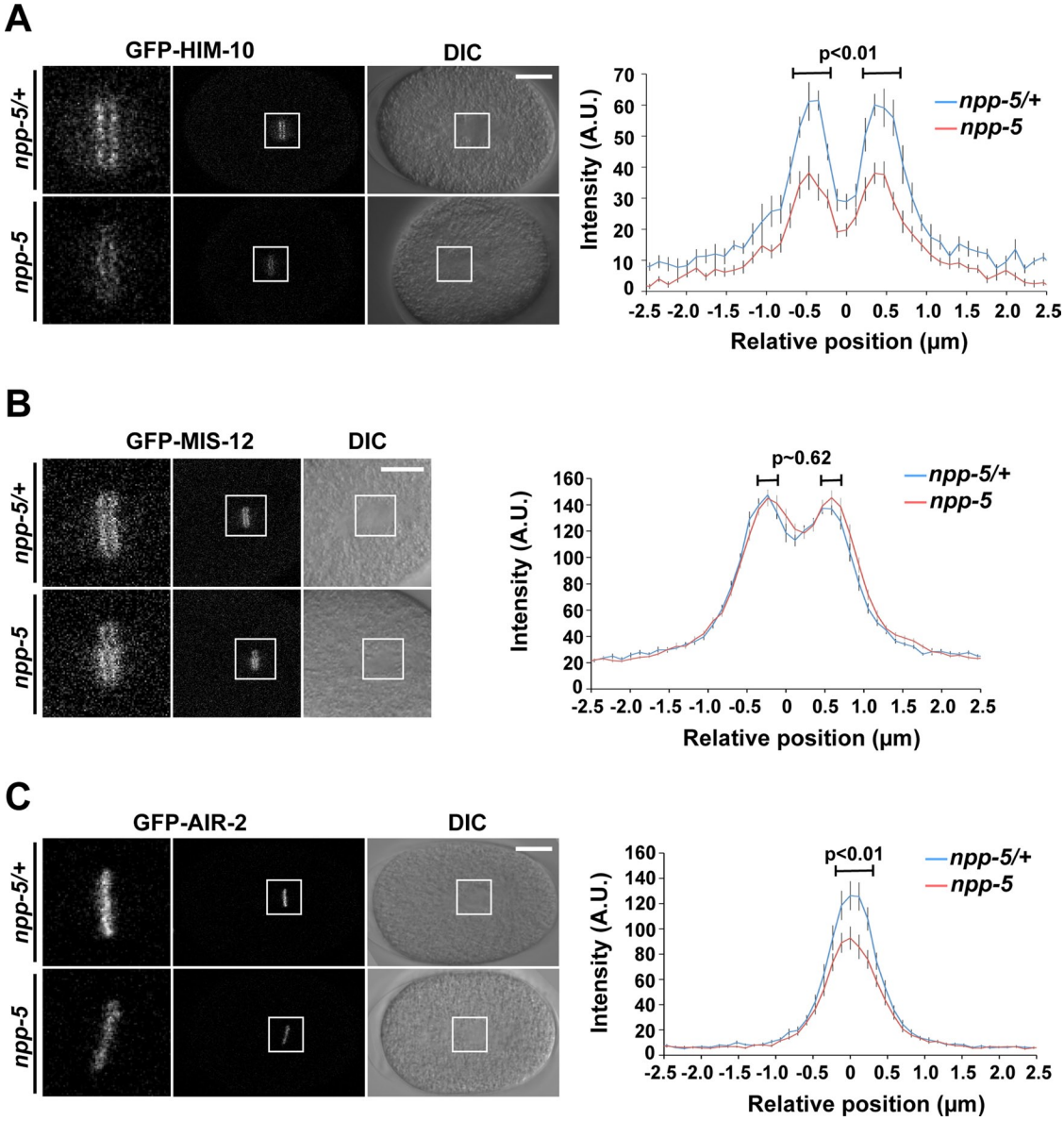

FIGURE 5: NPP-5 is required for efficient localization of HIM-10 and AIR-2. Still images from time-lapse confocal microscopy of control (*npp-5(tm3039)/+*) and *npp-5(tm3039)* embryos expressing GFP-HIM-10 (A), GFP-MIS-12 (B), or GFP-AIR-2 (C). Boxed regions (middle) are shown at higher magnification to the left. Scale bars, 10 μm. Graphs on the right represent mean fluorescence intensities measured in 5 × 2.3 μm^2 rectangles perpendicular to the metaphase plates. Position is relative to the center of metaphase chromosomes. Probability values (p) from two-tailed *t* tests are shown. Error bars, SE of the mean. n ≥ 15 in all experiments.

lethality phenotype specifically with the MDF-1/MDF-2 branch of the SAC.

The implication of NPP-5 in kinetochore assembly and AIR-2 localization suggested that chromatin segregation might be impaired in the absence of NPP-5. Moreover, the synthetic interaction of NPP-5 with MDF-1 and MDF-2 could reflect that these SAC proteins are required to prevent chromatin segregation defects in *npp-5(tm3039)* embryos by inducing an anaphase delay. Indeed, immunofluorescence analysis of *npp-5(tm3039)* mutants revealed chromatin bridges in 10% of the embryos ($p < 0.05$), a phenotype never observed in control embryos (Figure 8B). RNAi against *mdf-1* caused 5% chromatin bridges in control embryos, whereas a dramatic increase to 49% ($p < 0.001$) was observed upon depletion of MDF-1 from *npp-5(tm3039)* embryos. Thus MDF-1 is required to prevent chromosome missegregation in the absence of NPP-5.

It was recently found that loss of Cyclin B3/CYB-3 induces a strong SAC-dependent mitotic arrest (Deyter *et al.*, 2010), which we hypothesized might also require NPP-5. Because chromatin segregation is virtually abolished upon depletion of CYB-3 (Deyter *et al.*, 2010; our data not shown), we used other events to monitor mitotic progression: we defined "anaphase" on the basis of centrosome behavior and cleavage furrow ingression (~80 s after anaphase onset in control embryos). Compared to control embryos, time from pronuclear meeting (prophase) to anaphase was increased by 115% in embryos depleted for CYB-3 (Figure 8C; $p < 0.001$). Timing was unaffected in *npp-5* mutants incubated on control RNAi plates

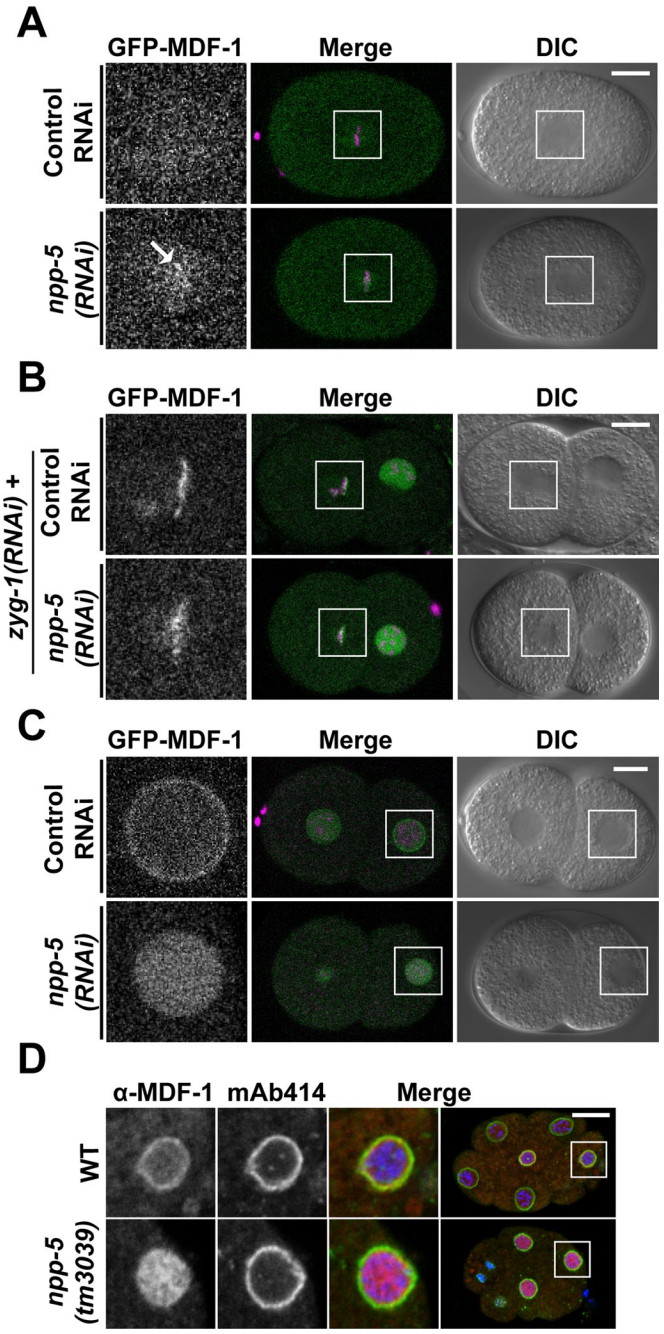

FIGURE 6: NPC localization of spindle assembly checkpoint protein MDF-1 depends on NPP-5. (A–C) Still images from time-lapse confocal microscopy of embryos expressing GFP-MDF-1 (green) and mCherry-HIS-58 (magenta). (A) Depletion of NPP-5 induces recruitment of GFP-MDF-1 to metaphase chromosomes (arrow; n = 10). (B) GFP-MDF-1 accumulation on chromosomes attached to monopolar spindles in *zyg-1(RNAi)* embryos is unaffected by depletion of NPP-5 (n = 3). (C) Localization of GFP-MDF-1 to NPCs in interphase is abolished in the absence of NPP-5 (n = 14). (D) Wild-type and *npp-5(tm3039)* embryos were fixed and stained with anti–MDF-1 antiserum (red) and mAb414 (green). Chromatin was detected using Hoechst 33258 (blue). Boxed regions in the merged panels are shown at higher magnification to the left. Scale bars, 10 μm.

(p = 0.10), but the *cyb-3(RNAi)*–induced mitotic delay was partially alleviated by removal of NPP-5 (17%; p = 0.01).

As an alternative way to test whether NPP-5 is required for proper SAC function, we examined response to oxygen deprivation. *C. elegans* embryos have a remarkable capacity to withstand anoxic stress. Under conditions of low oxygen, embryos arrest development and enter a stage known as suspended animation. This behavior is SAC dependent, implying a metaphase arrest, although cells may also be blocked in prophase (Nystul *et al.*, 2003; Hajeri *et al.*, 2010). To investigate whether embryos lacking NPP-5 are fully competent to enter suspended animation, we placed control and *npp-5(tm3039)* embryos under hypoxic conditions for 21 h before returning them to normal atmosphere. It is striking that, whereas the hypoxia stress only modestly decreased the frequency of control embryos completing embryogenesis and developing into fertile adults (2.4 and 7.5% decrease, respectively), the frequency of viable *npp-5(tm3039)* embryos decreased 13.3%, and only 1.1% of *npp-5(tm3039)* embryos developed into fertile adults following the hypoxia treatment (86.9% decrease; Figure 8D and Supplemental Table S1). This suggests that loss of NPP-5 sensitizes cells so they cannot withstand stress that otherwise would have been tolerated via SAC-induced mitotic arrest. From these results we conclude that NPP-5 is required for efficient cell cycle arrest under stress induced by either perturbation of cell cycle regulators or hypoxia.

DISCUSSION

Several studies determined that the NUP107 complex plays a crucial role in postmitotic and interphase NPC formation (Harel *et al.*, 2003; Walther *et al.*, 2003; D'Angelo *et al.*, 2006). Deeper understanding of the initial steps of NPC assembly has, however, been hindered by technical difficulties preventing the functional dissection of the NUP107 complex.

We provide here the first in vivo characterization of a metazoan NUP107 mutant. Moreover, we demonstrate that *C. elegans* NUP43/NPP-23, NUP85/NPP-2, and NUP133/NPP-15 localize at the nuclear periphery in interphase and at kinetochores during mitosis, thus behaving like bona fide NUP107 complex components. Previous depletion of NUP107 with siRNAs in HeLa cells or by immunoprecipitation from *Xenopus* extracts caused a codepletion of several NUP107 complex members, hampering a detailed understanding of how this ~720-kDa complex functions (Boehmer *et al.*, 2003; Harel *et al.*, 2003; Walther *et al.*, 2003). However, we show that the majority of Nups are expressed at normal levels in a *C. elegans NUP107*-null mutant, *npp-5(tm3039)*, paving the way to study the role of individual NUP107 complex members.

It is striking that, although most *npp-5* mutant animals do not complete development to adulthood, NPCs are formed, and neither nuclear protein import nor nuclear exclusion of soluble cytoplasmic content is grossly affected by the absence of NPP-5. The high lethality, in particular at 25°C, led us to conclude that *npp-5* is an essential gene in *C. elegans*, as also reported for *Schizosaccharomyces pombe* (Bai *et al.*, 2004) and *Drosophila melanogaster* (Katsani *et al.*, 2008). In contrast, deletion of the orthologous Nup84 gene from *S. cerevisiae* or *Aspergillus nidulans* causes milder, temperature-sensitive growth defects (Siniossoglou *et al.*, 1996; Osmani *et al.*, 2006).

Dissection of the Y-shaped NUP107 complex

Among Nups that belong to the NUP107 complex, we found that only NPP-23 and NPP-15 depend on NPP-5 for their correct localization. Recruitment of NPP-23 is diminished both at kinetochores during mitosis and at the NPC during interphase in the absence of NPP-5. The position of NUP43/NPP-23 within the Y-shaped NUP107 complex is unknown (Lutzmann *et al.*, 2002), but on the basis of our observation that other Nups are still at the NPC in the absence of NPP-5, we suggest that NPP-23 and NPP-5 may interact directly. On

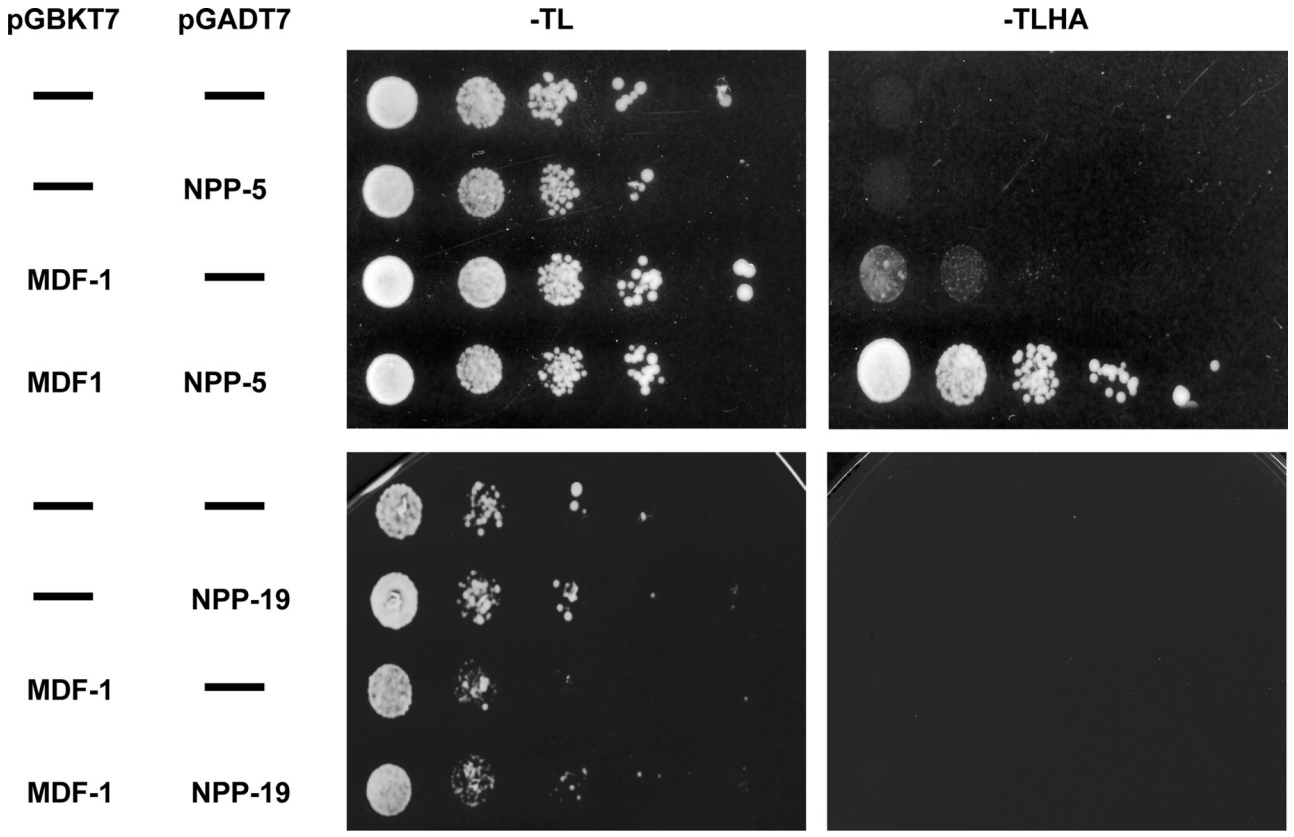

FIGURE 7: NPP-5 physically interacts with MDF-1 in yeast-two-hybrid assays. Full-length *npp-5* and *mdf-1* cDNAs were cloned into prey and bait vectors, respectively, and used to transform yeast cells. Growth on selective (–Trp-Leu-His-Ade) medium was only supported when the two genes were present together. No interaction was observed between NPP-19 and MDF-1.

the other hand, NPP-15 localizes normally at NPCs during interphase in *npp-5(tm3039)* embryos but does not localize at kinetochores in mitosis. The observation that NPC localization of endogenous NPP-15 is NPP-5 independent was unexpected since GFP-tagged human NUP133 mutated for the residues that mediate its interaction with NUP107 in vitro does not accumulate at the nuclear periphery in HeLa cells (Boehmer *et al.*, 2008). We propose that the addition of a GFP tag to NUP133 renders it more dependable on NUP107 for its NPC incorporation. Indeed, we observe that also *C. elegans* GFP-NPP-15 is dependent on NPP-5 for its localization to the NPC (Supplemental Figure S6). The position of NUP133 at the base of the Y-shaped complex "below" NUP107 (Lutzmann *et al.*, 2002) implies that removal of NUP107 should release NUP133 from the rest of the NUP107 complex. Thus, how does NPP-15 localize to the NPC in the absence of NPP-5? One possibility is that NPP-15 may interact physically with other Nups. In fact, it was recently suggested that the NUP107 complex is arranged in a head-to-tail manner within the NPC, through direct contacts between the NUP133 and Nup120p/NUP160, forming closed rings of eight NUP107 complexes (Seo *et al.*, 2009). Moreover, NUP133 contains an ALPS motif capable of sensing membrane curvature (Drin *et al.*, 2007), which plays a crucial role for NUP133 recruitment during de novo interphase NPC assembly (Doucet *et al.*, 2010). On the basis of these observations we propose that NUP133/NPP-15 may use several mechanisms for its NPC incorporation and that binding to NUP107/NPP-5 is only required for kinetochore targeting. It is interesting to note that Western blot analysis of *npp-5(tm3039)* extracts reveals only a single NPP-15 band, whereas two protein species are detected in wild-type extracts. We do not have information on the nature of the doublet in the wild type, but the differential behavior of NPP-15 in terms of NPC and kinetochore localization in the absence of NPP-5 leads us to speculate that the two NPP-15 bands represents different isoforms of NPP-15—one localizing to kinetochores during mitosis and another to NPCs during interphase in *C. elegans*. Without NPP-5 the former NPP-15 isoform becomes unstable, whereas the latter is stabilized through interactions with other Nups and/or pore membrane components. We found that depletion of other NUP107 complex proteins, such as NPP-2, NPP-10C, and NPP-6, efficiently abrogated NPP-5 recruitment and NPC assembly, suggesting that these proteins are critical for NUP107 complex stability and postmitotic NE reformation. An important conclusion from our work is therefore that the requirement for the NUP107 complex during NPC assembly is independent of NUP107/NPP-5 itself.

NPP-5 acts at multiple steps of mitosis

Although it is well established that NUP107/NPP-5 localizes to kinetochores in vertebrate and nematode cells (Belgareh *et al.*, 2001; Loiodice *et al.*, 2004; Franz *et al.*, 2005) but not in *Drosophila* (Katsani *et al.*, 2008), little is known about the functional implications. By depleting NUF2 from HeLa cells, Zuccolo and colleagues concluded that the NDC80 complex plays a major role in the recruitment of the NUP107 complex to kinetochores (Zuccolo *et al.*, 2007). Our observation that kinetochore accumulation of NUF2/HIM-10 is reduced in embryos lacking NPP-5 suggests that proper localization of the two protein complexes is interdependent. This is in contrast

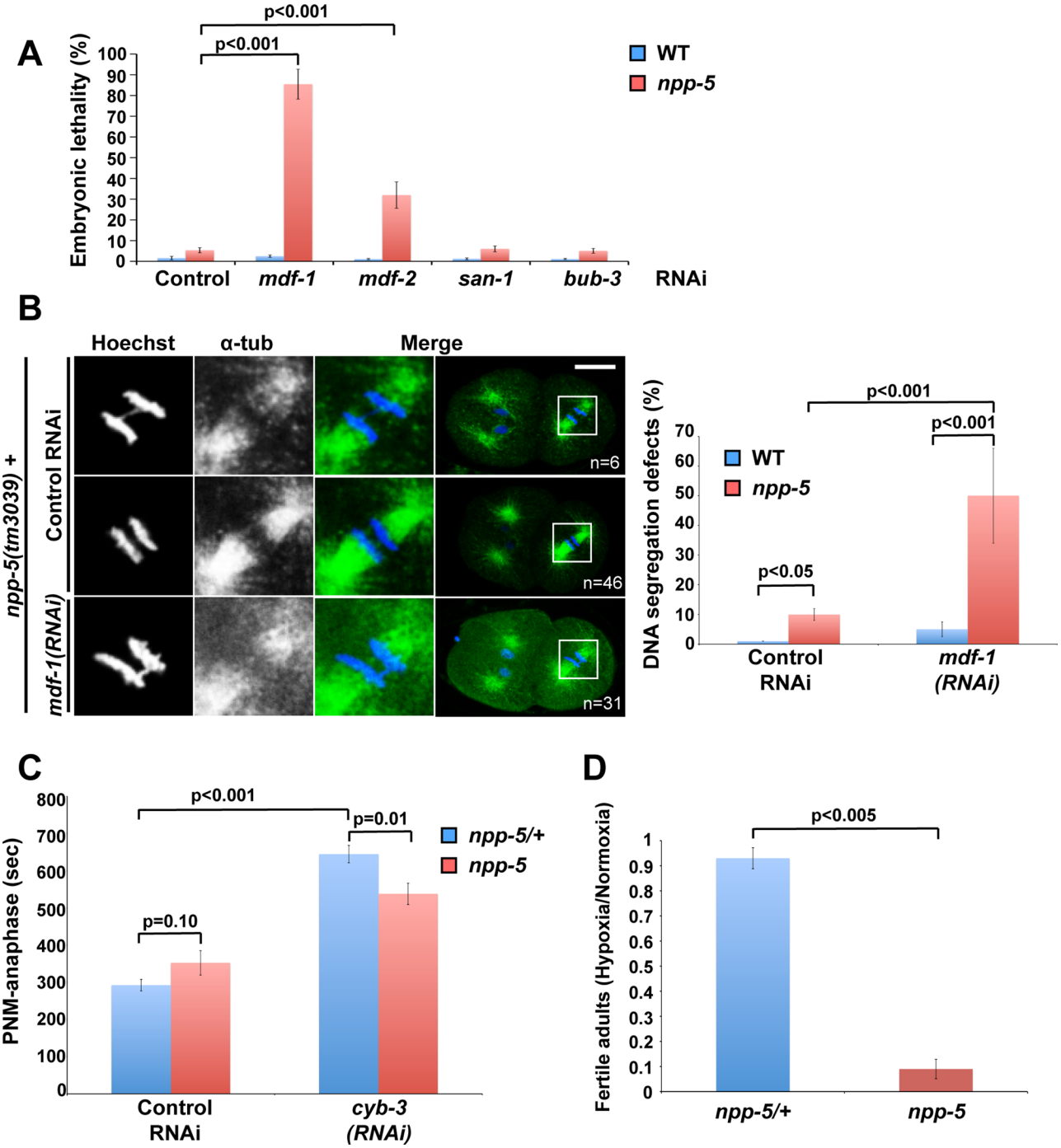

FIGURE 8: NPP-5 mutants are hypersensitive to MDF-1 depletion and anoxic stress. (A) Embryonic lethality was measured following RNAi against different members of the SAC in wild-type and *npp-5(tm3039)* animals (n > 600 embryos in all experiments). (B) Wild-type and *npp-5(tm3039)* animals treated with control or MDF-1 RNAi were fixed and stained with anti–α-tubulin (green). Chromatin was detected using Hoechst 33258 (blue). Boxed regions in the merged panels are shown at higher magnification to the left. Percentages of embryos presenting DNA segregation defects are indicated in the graph, demonstrating a synthetic phenotype in embryos simultaneously depleted for NPP-5 and MDF-1. (C) Time from pronuclear meeting (PNM) to anaphase was measured following incubation on control or *cyb-3* RNAi plates for 30 h (n ≥ 5 for all treatments). (D) Embryos from *npp-5(tm3039)/+* and *npp-5(tm3039)* animals were exposed to hypoxia for 21 h. After recovery under normoxic conditions development into fertile adults was determined, revealing a severe effect in *npp-5(tm3039)* mutants (n > 600 embryos in all experiments). Probability values (p) are shown from chi-square tests (A, B), two-tailed *t* test (C), and Wilcoxon rank sum test (D). Error bars, SE of the mean.

to the experiments of Zuccolo and colleagues, in which inhibition of NUP107 complex recruitment to kinetochores through *SEH1* siRNA treatment did not affect localization of HEC1, which forms heterodimers with NUF2 (Zuccolo *et al.*, 2007). However, since detectable levels of SEH1 were still present upon siRNA treatment, we propose that residual NUP107 complex activity at kinetochores was sufficient

for the HEC1 accumulation observed by Zuccolo and coworkers, whereas complete absence of NPP-5 causes a ~40% decrease in HIM-10 as reported here. Of importance, MIS-12 localized normally in *npp-5(tm3039)* embryos, which suggest that NPP-5 acts at specific steps of kinetochore assembly.

Our observation that 10% of dividing *npp-5(tm3039)* embryos contained lagging chromosomes during mitosis is compatible with reduced correction of syntelic microtubule–kinetochore attachments by Aurora B/AIR-2 (Lampson and Cheeseman, 2011), as also proposed for *SEH1*-depleted HeLa cells (Platani *et al.*, 2009). Moreover, alterations in kinetochore structure upon NPP-5 depletion, including reduced HIM-10 accumulation, are likely to be detected by the SAC. Indeed, we observed accumulation of GFP-MAD1/MDF-1 on mitotic chromosomes in embryos depleted for NPP-5, as also reported upon interfering with kinetochore localization of the entire NUP107 complex though depletion of SEH1 in HeLa cells (Zuccolo *et al.*, 2007). Finally, *npp-5(tm3039)*-mutant embryos were hypersensitive to depletion of MDF-1, resulting in 85% embryonic lethality and lagging chromosomes in 49% of dividing cells, which further supports the possibility that the SAC is responsible for detection and correction of mitotic spindle defects caused by the absence of NPP-5.

Our experiments unexpectedly revealed that MDF-1 depends strictly on NPP-5 in order to accumulate at the nuclear periphery during interphase. MAD1 localization to NPCs was previously described in different organisms, but a clear functional implication of this behavior is lacking. In *S. cerevisiae* the interaction with the NPC is mediated via Nup53p and Mlp1p/Mlp2p (Scott *et al.*, 2005), whereas in HeLa cells localization of MAD1 to the NPC is dependent on the Mlp1p/Mlp2p homologue TPR (Lee *et al.*, 2008) and NUP153 (Lussi *et al.*, 2010). Yeast-two-hybrid experiments presented here demonstrate that *C. elegans* MDF-1 interacts directly with NPP-5 but not with NUP35/NPP-19. Thus our data show that accumulation of MAD1 at NPCs is conserved and that different MAD1–Nup interactions may have arisen during evolution.

Cells are more dependent on the SAC in situations of stress. Our observation that suspended animation and delay in mitotic progression were compromised in the absence of NPP-5, combined with the genetic and physical interaction between NPP-5 and MDF-1, suggests that NPP-5 may play an active role in control of chromosome segregation and cell cycle progression. We propose that NUP107/NPP-5 may serve as binding site for MAD1/MDF-1 both at the NPC and at kinetochores and that the two proteins may even translocate together at the entry into mitosis. However, future experiments are required to analyze this interaction in further detail.

MATERIALS AND METHODS

Nematode strains and transgenesis

The wild-type strain used was the *C. elegans* Bristol strain N2. BN51 *bqIs51*[$P_{pie\text{-}1}$*::gfp::npp-5*] and XA3545 *qaIs3545*[$P_{pie\text{-}1}$*::gfp::him-10*] were obtained by microparticle bombardment (Praitis *et al.*, 2001) of DP38 using either plasmid pUP1 or plasmids pPAG27 and pDP#MM051, respectively. BN128 *bqEx128*[$P_{npp\text{-}2}$*::gfp::npp-2;* $P_{lmn\text{-}1}$*::mCherry::his-58*] was obtained by microinjection of plasmids pBN1 and pBN29 into N2. BN150 *bqSi150*[$P_{hsp\text{-}16.41}$*::gfp::C09G9.2a*] and BN168 bqSi168[$P_{hsp\text{-}16.41}$*::gfp::npp-15*] were obtained by MosSCI transformation (Frokjaer-Jensen *et al.*, 2008) of EG4322 with plasmids pBN27 and pBN23, respectively. BN68 *bqIs51*[$P_{pie\text{-}1}$*::gfp::npp-5*]; *ltIs37*[$P_{pie\text{-}1}$*::mCherry::his-58*] was made by crossing BN51 and OD57 (McNally *et al.*, 2006). *npp-5(tm3039)* was provided by Shohei Mitani of the Japanese National Bioresource Project (Tokyo, Japan) and backcrossed to the wild type six times before balancing to obtain strain BN40. *npp-5(ok1966)* was provided by the International *C. elegans* Gene Knockout Consortium (http://celeganskoconsortium.omrf.org/) and backcrossed to the wild type six times to obtain the homozygous strain BN28 and the balanced strain BN85. Subsequently, BN40 was crossed with the following strains: TJ356 (Henderson and Johnson, 2001) to generate BN22 *npp-5(tm3039)/mIn1*; *zIs356*[*daf-16::gfp*]; BN68 to generate BN69 *npp-5(tm3039)/mIn1*; *bqIs51*[$P_{pie\text{-}1}$*::gfp::npp-5*]; *ltIs37*[$P_{pie\text{-}1}$*::mCherry::his-58*]; JH1327 (Reese *et al.*, 2000) to generate BN73 *npp-5(tm3039)/mIn1*; *axIs*[$P_{pie\text{-}1}$*::pie-1::gfp*]; XA3501 (Askjaer *et al.*, 2002) to generate BN106 *npp-5(tm3039)/mIn1*; *ruIs32*[$P_{pie\text{-}1}$*::gfp::his-58*]; XA3545 to generate BN114 *npp-5(tm3039)/mIn1*; *qaIs3545*[$P_{pie\text{-}1}$*::gfp::him-10*]; BN128 to generate BN133 *npp-5(tm3039)/mIn1*; *bqEx128*[$P_{npp\text{-}2}$*::gfp::npp-2;* $P_{lmn\text{-}1}$*::mCherry::his-58*]; OD27 (CGC) to generate BN153 *npp-5(tm3039)/mIn1*; *ltIs14*[$P_{pie\text{-}1}$*::gfp::air-2*]; and OD8 (Cheeseman *et al.*, 2004) to generate BN159 *npp-5(tm3039)/mIn1*; *ltIs4*[$P_{pie\text{-}1}$*::gfp::mis-12*]. Similarly, BN28 was crossed with PS3808 (Gupta and Sternberg, 2002) to generate BN59 *npp-5(ok1966)*; *syIs80*[*Plin-11::nls::gfp::lacZ*]. *npp-15(ok1954)* was provided by the International *C. elegans* Gene Knockout Consortium and backcrossed to the wild type six times before balancing to obtain strain BN126. RQ244 *mdf-1(gk2)* V; *jzIs1*[$P_{pie\text{-}1}$*::gfp:: mdf-1*]; *ltIs37*[$P_{pie\text{-}1}$*::mCherry::his-58*] and OD110 ltIs52[$P_{pie\text{-}1}$*::gfp::mdf-2*] *ltIs37*[$P_{pie\text{-}1}$*::mCherry::his-58*] were as described (Yamamoto *et al.*, 2008; Essex *et al.*, 2009). For further details on strains refer to Supplemental Table S2. All strains were cultured using standard *C. elegans* methods (Stiernagle, 2006).

Plasmids and RNAi

Plasmid pQE30-NPP-15 (amino acids 739–1024) for expression of hexahistidine-tagged NPP-15 antigen was generated by PCR amplification of *C. elegans* genomic DNA (primers B153 + B154). Plasmid pUP1 for expression of GFP-NPP-5 was made by insertion of *unc-119* derived from plasmid pDP#MM051 (Maduro and Pilgrim, 1995) into pPAG1 (Franz *et al.*, 2005). Plasmid pPAG27 for expression of GFP-HIM-10 was constructed by replacing the *lmn-1* gene of plasmid pPAG4 (Galy *et al.*, 2003) with a PCR-amplified *him-10* sequence (primers H556 + H557). Plasmid pBN29 for expression of GFP-NPP-2 was generated by cloning the *npp-2* gene (primers B069 + B200 + B071 + B072) into plasmid pBN8, a derivative of pCFJ151 (Frokjaer-Jensen *et al.*, 2008) containing a longer polylinker. pBN29 includes 1993 base pairs upstream of the start codon and 560 base pairs downstream of the stop codon, as well as GFP inserted into a PCR-engineered *Bsr*GI site immediately after the start codon. Plasmids pBN23 and pBN27 for expression of GFP-NPP-15 and GFP-NPP-23 were generated by cloning *npp-15* (primers B236 + B237) and C09G9.2a (primers B248 + B249) into plasmid pBN16, respectively. Plasmid pBN16 for single-copy integration of heat shock–inducible transgenes into the *C. elegans* genome was made by insertion of the *hsp-16.41* promoter (primers B216 + B232), a polylinker, and the *unc-54 3'* untranslated region (UTR; B233 + B217) into pBN8. Plasmid pBN1 for expression of mCherry-HisH2B in somatic cells contains the *lmn-1* promoter (5088 base pairs) in front of a *mCherry-his-58* fusion gene and the *pie-1* 3'UTR (1822 base pairs).

Plasmids pGADT7-*npp-5* and pAD-*npp-19* encoding the yeast Gal4 activation domain fused to either *C. elegans* NPP-5 or NPP-19 were constructed by RT-PCR amplification with primers B364 + B366 and primers H624 + H633, respectively. Plasmid pGBKT7-*mdf-1* encoding the yeast Gal4 DNA–binding domain fused to *C. elegans* MDF-1 was constructed by PCR amplification of *mdf-1* cDNA from plasmid pACT-Ptac-GST (Watanabe *et al.*, 2008), using primers B367 + B368 into pGBKT7 (Clontech, Mountain View, CA).

For primer sequences refer to Supplemental Table S3. All constructions were verified by sequencing.

RNAi constructs were described previously (Galy *et al.*, 2003; Kamath *et al.*, 2003). The empty pPD129.36 vector was used as negative control. RNAi experiments were performed by feeding at 20°C for ~36 h unless otherwise specified (Galy *et al.*, 2003).

Production and purification of antibodies

NPP-5 and NPP-15 antibodies were raised in rabbits against a synthetic NPP-5 peptide (amino acids 11–26) and recombinant NPP-15 (amino acids 738–1023), respectively. Antibodies were affinity purified from sera using either an Affi-Gel 15 (Bio-Rad, Hercules, CA) column coupled with the synthetic NPP-5 peptide or Immobilon-P (Millipore, Billerica, MA) membrane coated with the NPP-15 antigen. Bound antibodies were eluted with 0.1 M glycine (pH 2.5) and immediately neutralized with 1 M Tris (pH 8.0).

Dextran microinjection and live embryo imaging

Fluorescein isothiocyanate–labeled, 70-kDa dextran (FD70S; Sigma-Aldrich, St. Louis, MO) and tetramethylrhodamine isothiocyanate–labeled, 155-kDa dextran (T1287; Sigma-Aldrich) were purified using a Nanosep 10K centrifugal device (OD010C33; Nanosep, Lund, Sweden) until a final concentration of 2 mg/ml in phosphate-buffered saline (PBS). A 1:1 mixture of the two dextrans was injected into the gonads of N2 and BN40 animals, followed by incubation at 20°C for 5 h before dissection.

Fluorescent reporters driven by the *hsp-16.41* promoter were induced by a 32.7°C heat shock for 15 min, followed by 5-h recovery at 20°C prior to observation.

Embryos were mounted in M9 buffer (86 mM NaCl, 22 mM KH_2PO_4, 34 mM Na_2HPO_4, 1 mM $MgSO_4$) between a coverslip and a 2% agarose pad. Epifluorescence and transmitted light were recorded at 22–24°C with a Leica confocal TCS SP2 microscope through an HCX PL APO 63×/1.4 objective (Leica, Wetzlar, Germany). Images were captured using integrated Leica software and processed with ImageJ (National Institutes of Health, Bethesda, MD) and Adobe Photoshop (Adobe, San Jose, CA). The laser intensity was adjusted so that no effect on development was observed. Images were collected at 20-s intervals for a total of 20–40 min, except for Figure 5B, where images were collected at 5-s intervals.

Immunofluorescence

Gravid hermaphrodites were dissected in 3 µl of M9 buffer directly on poly-L-lysine–coated glass slides and covered with 12 × 12 mm coverslips. To crack the eggshells, slides were transferred immediately to metal plates on top of dry ice. After 15 min, coverslips were flicked off and slides were placed in methanol for 15–18 min at −18°C. After rehydration for 30 min in PBS with 0.1% Tween 20 (PBST) and blocking for 30 min with 10% fetal calf serum in PBST (PBST-F) the embryos were incubated for 2 h with primary antibodies diluted in PBST-F as indicated in Supplemental Table S4. Embryos were washed for 1 h in PBST, followed by incubation for 2 h with secondary antibodies diluted in PBST-F. Secondary antibodies were Alexa Fluor 546–conjugated goat anti-mouse antibodies (1:1000; Invitrogen, Carlsbad, CA) and Alexa Fluor 633–conjugated goat anti-rabbit antibodies (1:1000; Invitrogen). Embryos were washed again for 1 h in PBST and finally mounted with Mowiol containing 5 µg/ml Hoechst 33258. All steps were at room temperature. Confocal images were obtained with a Leica confocal SPE microscope equipped with a ACS APO 63×/1.3 objective and processed with ImageJ and Adobe Photoshop.

Western Blot

Embryos were obtained by hypochlorite treatment (1 N NaOH, 30% bleach solution) and disrupted by boiling and vortexing in SDS sample buffer together with 0.5-µm-diameter glass beads and separated by 10% SDS–PAGE. Proteins were transferred to Immobilon P membranes (Millipore), which were blocked with PBS containing 0.05% Tween-20 and 3% low-fat milk (PBST-M) and probed for 2 h at room temperature with antibodies diluted in PBST-M as described in Supplemental Table S4. Next membranes were washed with PBST for 1 h, incubated with peroxidase-conjugated secondary antibodies (1:5000–1:10,000; Sigma-Aldrich) for 2 h at room temperature, and developed with ECL Plus (GE Amersham, Piscataway, NJ).

Anoxia experiments

Ten gravid young hermaphrodites per condition were placed on a nematode growth medium plate for 1 h to lay embryos. The hermaphrodites were removed, and plates were placed in an anaerobic jar (Schütt Labortechnik, Göttingen, Germany) that was flushed with nitrogen gas (O2 < 0.1%). After 21 h at 20°C, plates were removed from the jar, and development was monitored for 4 d.

Yeast-two-hybrid assay

Yeast strain AH109 (Clontech; *MATa, trp1-901, leu2-3, 112, ura3-52, his3-200, gal4?, gal80?, LYS2::GAL1$_{UAS}$-GAL1$_{TATA}$-HIS3, GAL2$_{UAS}$-GAL2$_{TATA}$-ADE2, URA3::MEL1$_{TATA}$-lacZ*) was transformed using the LiAc method and selected in the appropriate synthetic complete (SC) minimal medium. Transformants containing pGBKT7-*mdf-1* and either pGADT7-*npp-5* or pAD-*npp-19* were grown at 30°C to OD600 0.5 in SC-Leu-Trp medium and spotted as 10-fold serial dilutions to detect the ability to grow on minimal-medium plates lacking adenine and histidine. Growth was assayed after 3 d at 30°C. Combinations of empty pGADT7 and pGBKT7 vectors were also transformed into AH109 with each construct to assess self-activation.

ACKNOWLEDGMENTS

We thank A. Arroyo, A. Desai, K. Kemphues, R. Kitagawa, and C. Luque for reagents and P. Alarcón and M. Rodríguez for technical assistance. V. Galy, A. Miranda-Vizuete, J. R. Martínez-Morales, and members of the Askjaer lab are acknowledged for discussion on the manuscript. This work was funded by the Spanish Ministry of Science and Innovation (BFU-2007-60116, BFU-2010-15478), the Spanish National Research Council (200820I028), the European Regional Development Fund, and the Regional Government of Andalusia (P07-CVI-02697). In addition, we acknowledge the Fundación Ramón Areces for a fellowship to E.R. and the Junta de Andalucía for institutional support. Some nematode strains used in this work were provided by the National Bioresource Project for the Nematode *C. elegans* (directed by Shohei Mitani), the *C. elegans* Gene Knockout Consortium, and the *Caenorhabditis* Genetic Center (University of Minnesota, Minneapolis, MN), which is funded by the National Institutes of Health, National Center for Research Resources.

REFERENCES

Alber F *et al.* (2007). The molecular architecture of the nuclear pore complex. Nature 450, 695–701.

Askjaer P, Galy V, Hannak E, Mattaj IW (2002). Ran GTPase cycle and importins alpha and beta are essential for spindle formation and nuclear envelope assembly in living *Caenorhabditis elegans* embryos. Mol Biol Cell 13, 4355–4370.

Bai SW, Rouquette J, Umeda M, Faigle W, Loew D, Sazer S, Doye V (2004). The fission yeast Nup107-120 complex functionally interacts with the

small GTPase Ran/Spi1 and is required for mRNA export, nuclear pore distribution, and proper cell division. Mol Cell Biol 24, 6379–6392.
Belgareh N *et al.* (2001). An evolutionarily conserved NPC subcomplex, which redistributes in part to kinetochores in mammalian cells. J Cell Biol 154, 1147–1160.
Boehmer T, Enninga J, Dales S, Blobel G, Zhong H (2003). Depletion of a single nucleoporin, Nup107, prevents the assembly of a subset of nucleoporins into the nuclear pore complex. Proc Natl Acad Sci USA 100, 981–985.
Boehmer T, Jeudy S, Berke IC, Schwartz TU (2008). Structural and functional studies of Nup107/Nup133 interaction and its implications for the architecture of the nuclear pore complex. Mol Cell 30, 721–731.
Campbell MS, Chan GK, Yen TJ (2001). Mitotic checkpoint proteins HsMAD1 and HsMAD2 are associated with nuclear pore complexes in interphase. J Cell Sci 114, 953–963.
Capelson M, Liang Y, Schulte R, Mair W, Wagner U, Hetzer MW (2010). Chromatin-bound nuclear pore components regulate gene expression in higher eukaryotes. Cell 140, 372–383.
Cheeseman IM, Desai A (2008). Molecular architecture of the kinetochore-microtubule interface. Nat Rev Mol Cell Biol 9, 33–46.
Cheeseman IM, Niessen S, Anderson S, Hyndman F, Yates JR 3rd, Oegema K, Desai A (2004). A conserved protein network controls assembly of the outer kinetochore and its ability to sustain tension. Genes Dev 18, 2255–2268.
Cronshaw JM, Krutchinsky AN, Zhang W, Chait BT, Matunis MJ (2002). Proteomic analysis of the mammalian nuclear pore complex. J Cell Biol 158, 915–927.
D'Angelo MA, Anderson DJ, Richard E, Hetzer MW (2006). Nuclear pores form de novo from both sides of the nuclear envelope. Science 312, 440–443.
D'Angelo MA, Raices M, Panowski SH, Hetzer MW (2009). Age-dependent deterioration of nuclear pore complexes causes a loss of nuclear integrity in postmitotic cells. Cell 136, 284–295.
Deyter GM, Furuta T, Kurasawa Y, Schumacher JM (2010). *Caenorhabditis elegans* cyclin B3 is required for multiple mitotic processes including alleviation of a spindle checkpoint-dependent block in anaphase chromosome segregation. PLoS Genet 6, e1001218.
Doucet CM, Talamas JA, Hetzer MW (2010). Cell cycle-dependent differences in nuclear pore complex assembly in metazoa. Cell 141, 1030–1041.
Drin G, Casella JF, Gautier R, Boehmer T, Schwartz TU, Antonny B (2007). A general amphipathic alpha-helical motif for sensing membrane curvature. Nat Struct Mol Biol 14, 138–146.
Essex A, Dammermann A, Lewellyn L, Oegema K, Desai A (2009). Systematic analysis in *Caenorhabditis elegans* reveals that the spindle checkpoint is composed of two largely independent branches. Mol Biol Cell 20, 1252–1267.
Fang G, Yu H, Kirschner MW (1998). Direct binding of CDC20 protein family members activates the anaphase-promoting complex in mitosis and G1. Mol Cell 2, 163–171.
Franz C, Askjaer P, Antonin W, Iglesias CL, Haselmann U, Schelder M, de Marco A, Wilm M, Antony C, Mattaj IW (2005). Nup155 regulates nuclear envelope and nuclear pore complex formation in nematodes and vertebrates. EMBO J 24, 3519–3531.
Frokjaer-Jensen C, Davis MW, Hopkins CE, Newman BJ, Thummel JM, Olesen SP, Grunnet M, Jorgensen EM (2008). Single-copy insertion of transgenes in *Caenorhabditis elegans*. Nat Genet 40, 1375–1383.
Galy V, Askjaer P, Franz C, Lopez-Iglesias C, Mattaj IW (2006). MEL-28, a novel nuclear-envelope and kinetochore protein essential for zygotic nuclear-envelope assembly in *C. elegans*. Curr Biol 16, 1748–1756.
Galy V, Mattaj IW, Askjaer P (2003). *Caenorhabditis elegans* nucleoporins Nup93 and Nup205 determine the limit of nuclear pore complex size exclusion in vivo. Mol Biol Cell 14, 5104–5115.
Gorjanacz M, Jaedicke A, Mattaj IW (2007). What can *Caenorhabditis elegans* tell us about the nuclear envelope? FEBS Lett 581, 2794–2801.
Grandi P, Dang T, Pane N, Shevchenko A, Mann M, Forbes D, Hurt E (1997). Nup93, a vertebrate homologue of yeast Nic96p, forms a complex with a novel 205-kDa protein and is required for correct nuclear pore assembly. Mol Biol Cell 8, 2017–2038.
Gupta BP, Sternberg PW (2002). Tissue-specific regulation of the LIM homeobox gene lin-11 during development of the *Caenorhabditis elegans* egg-laying system. Dev Biol 247, 102–115.
Hajeri VA, Little BA, Ladage ML, Padilla PA (2010). NPP-16/Nup50 function and CDK-1 inactivation are associated with anoxia-induced prophase arrest in *Caenorhabditis elegans*. Mol Biol Cell 21, 712–724.
Harel A, Orjalo AV, Vincent T, Lachish-Zalait A, Vasu S, Shah S, Zimmerman E, Elbaum M, Forbes DJ (2003). Removal of a single pore subcomplex results in vertebrate nuclei devoid of nuclear pores. Mol Cell 11, 853–864.
Henderson ST, Johnson TE (2001). *daf-16* integrates developmental and environmental inputs to mediate aging in the nematode *Caenorhabditis elegans*. Curr Biol 11, 1975–1980.
Hetzer MW, Wente SR (2009). Border control at the nucleus: biogenesis and organization of the nuclear membrane and pore complexes. Dev Cell 17, 606–616.
Iouk T, Kerscher O, Scott RJ, Basrai MA, Wozniak RW (2002). The yeast nuclear pore complex functionally interacts with components of the spindle assembly checkpoint. J Cell Biol 159, 807–819.
Kalverda B, Pickersgill H, Shloma VV, Fornerod M (2010). Nucleoporins directly stimulate expression of developmental and cell-cycle genes inside the nucleoplasm. Cell 140, 360–371.
Kamath RS *et al.* (2003). Systematic functional analysis of the *Caenorhabditis elegans* genome using RNAi. Nature 421, 231–237.
Katsani KR, Karess RE, Dostatni N, Doye V (2008). In vivo dynamics of *Drosophila* nuclear envelope components. Mol Biol Cell 19, 3652–3666.
Lampson MA, Cheeseman IM (2011). Sensing centromere tension: Aurora B and the regulation of kinetochore function. Trends Cell Biol 21, 133–140.
Lee SH, Sterling H, Burlingame A, McCormick F (2008). Tpr directly binds to Mad1 and Mad2 and is important for the Mad1-Mad2-mediated mitotic spindle checkpoint. Genes Dev 22, 2926–2931.
Loiodice I, Alves A, Rabut G, Van Overbeek M, Ellenberg J, Sibarita JB, Doye V (2004). The entire Nup107-160 complex, including three new members, is targeted as one entity to kinetochores in mitosis. Mol Biol Cell 15, 3333–3344.
Lussi YC, Shumaker DK, Shimi T, Fahrenkrog B (2010). The nucleoporin Nup153 affects spindle checkpoint activity due to an association with Mad1. Nucleus 1, 71–84.
Lutzmann M, Kunze R, Buerer A, Aebi U, Hurt E (2002). Modular self-assembly of a Y-shaped multiprotein complex from seven nucleoporins. EMBO J 21, 387–397.
Maduro M, Pilgrim D (1995). Identification and cloning of unc-119, a gene expressed in the *Caenorhabditis elegans* nervous system. Genetics 141, 977–988.
Maresca TJ, Salmon ED (2009). Intrakinetochore stretch is associated with changes in kinetochore phosphorylation and spindle assembly checkpoint activity. J Cell Biol 184, 373–381.
McNally K, Audhya A, Oegema K, McNally FJ (2006). Katanin controls mitotic and meiotic spindle length. J Cell Biol 175, 881–891.
Nystul TG, Goldmark JP, Padilla PA, Roth MB (2003). Suspended animation in *C. elegans* requires the spindle checkpoint. Science 302, 1038–1041.
Orjalo AV, Arnaoutov A, Shen Z, Boyarchuk Y, Zeitlin SG, Fontoura B, Briggs S, Dasso M, Forbes DJ (2006). The Nup107-160 nucleoporin complex is required for correct bipolar spindle assembly. Mol Biol Cell 17, 3806–3818.
Osmani AH, Davies J, Liu HL, Nile A, Osmani SA (2006). Systematic deletion and mitotic localization of the nuclear pore complex proteins of *Aspergillus nidulans*. Mol Biol Cell 17, 4946–4961.
Platani M, Santarella-Mellwig R, Posch M, Walczak R, Swedlow JR, Mattaj IW (2009). The Nup107-160 nucleoporin complex promotes mitotic events via control of the localization state of the chromosome passenger complex. Mol Biol Cell 20, 5260–5275.
Praitis V, Casey E, Collar D, Austin J (2001). Creation of low-copy integrated transgenic lines in *Caenorhabditis elegans*. Genetics 157, 1217–1226.
Reese KJ, Dunn MA, Waddle JA, Seydoux G (2000). Asymmetric segregation of PIE-1 in *C. elegans* is mediated by two complementary mechanisms that act through separate PIE-1 protein domains. Mol Cell 6, 445–455.
Rodenas E, Klerkx EP, Ayuso C, Audhya A, Askjaer P (2009). Early embryonic requirement for nucleoporin Nup35/NPP-19 in nuclear assembly. Dev Biol 327, 399–409.
Rout MP, Aitchison JD, Suprapto A, Hjertaas K, Zhao Y, Chait BT (2000). The yeast nuclear pore complex: composition, architecture, and transport mechanism. J Cell Biol 148, 635–651.
Scott RJ, Lusk CP, Dilworth DJ, Aitchison JD, Wozniak RW (2005). Interactions between Mad1p and the nuclear transport machinery in the yeast *Saccharomyces cerevisiae*. Mol Biol Cell 16, 4362–4374.
Seo HS, Ma Y, Debler EW, Wacker D, Kutik S, Blobel G, Hoelz A (2009). Structural and functional analysis of Nup120 suggests ring formation of the Nup84 complex. Proc Natl Acad Sci USA 106, 14281–14286.
Siniossoglou S, Lutzmann M, Santos-Rosa H, Leonard K, Mueller S, Aebi U, Hurt E (2000). Structure and assembly of the Nup84p complex. J Cell Biol 149, 41–54.

Siniossoglou S, Wimmer C, Rieger M, Doye V, Tekotte H, Weise C, Emig S, Segref A, Hurt EC (1996). A novel complex of nucleoporins, which includes Sec13p and a Sec13p homolog, is essential for normal nuclear pores. Cell 84, 265–275.

Stiernagle T (2006). Maintenance of *C. elegans*. In WormBook. The Online Review of *C. elegans* Biology. http://www.wormbook.org/chapters/www_strainmaintain/strainmaintain.html.

Strambio-De-Castillia C, Niepel M, Rout MP (2010). The nuclear pore complex: bridging nuclear transport and gene regulation. Nat Rev Mol Cell Biol 11, 490–501.

Tanaka TU (2010). Kinetochore-microtubule interactions: steps towards bi-orientation. EMBO J 29, 4070–4082.

Theerthagiri G, Eisenhardt N, Schwarz H, Antonin W (2010). The nucleoporin Nup188 controls passage of membrane proteins across the nuclear pore complex. J Cell Biol 189, 1129–1142.

Uchida KS, Takagaki K, Kumada K, Hirayama Y, Noda T, Hirota T (2009). Kinetochore stretching inactivates the spindle assembly checkpoint. J Cell Biol 184, 383–390.

Walther TC *et al*. (2003). The conserved Nup107-160 complex is critical for nuclear pore complex assembly. Cell 113, 195–206.

Wan X *et al*. (2009). Protein architecture of the human kinetochore microtubule attachment site. Cell 137, 672–684.

Watanabe S, Yamamoto TG, Kitagawa R (2008). Spindle assembly checkpoint gene *mdf-1* regulates germ cell proliferation in response to nutrition signals in *C. elegans*. EMBO J 27, 1085–1096.

Yamamoto TG, Watanabe S, Essex A, Kitagawa R (2008). SPDL-1 functions as a kinetochore receptor for MDF-1 in *Caenorhabditis elegans*. J Cell Biol 183, 187–194.

Zuccolo M *et al*. (2007). The human Nup107-160 nuclear pore subcomplex contributes to proper kinetochore functions. EMBO J 26, 1853–1864.